Combustion and Flame 232 (2021) 111535

Contents lists available at ScienceDirect

Combustion and Flame

journal homepage: www.elsevier.com/locate/combustflame

One-dimensional dynamics of gaseous detonations revisited

Hassan Tofaili[a], Guido Lodato[a], Luc Vervisch[a,*], Paul Clavin[b]

[a] Normandie Université, CNRS, INSA Rouen Normandie, CORIA UMR6614, Saint-Etienne-du-Rouvray 76801, France
[b] Aix Marseille Université, CNRS, Centrale Marseille, IRPHE UMR7342, Marseille 13384, France

ARTICLE INFO

Article history:
Received 23 February 2021
Revised 28 May 2021
Accepted 28 May 2021

Keywords:
Detonation
Compressible reaction-wave stability
Asymptotic analysis
High-order simulation methods

ABSTRACT

Stability of one-dimensional gaseous detonations is revisited using both asymptotic analysis and high-order numerical simulations. The double limit of small heat release and a ratio of specific heats close to unity is considered, and attention is focused on weakly unstable detonations in the Chapman-Jouguet regime. It is shown that the time-dependent velocity of the lead shock can be obtained as the eigenfunction of a hyperbolic problem reducing to a single hyperbolic equation for the flow. The solution is then expressed in the form of an integral equation for the shock velocity, from which the threshold activation energy for transition to instability and the oscillation frequency can be obtained. These theoretical findings are validated against a set of direct numerical simulations of one-dimensional detonations in the same limit, performed using a high-order spectral difference scheme in which particular care is taken to ensure a high resolution of the flow with minimal numerical dissipation, while also suppressing post-shock numerical aberrations. Values of detonation parameters at the instability threshold obtained from numerical simulations are systematically compared against their theoretical counterparts, confirming the validity of the proposed asymptotic theory.

1. Introduction

Starting with the early works by Erpenbeck [1] and Fickett and Wood [2] back in the 1960s, the dynamics of detonation waves has been subject to numerous experimental, theoretical and numerical studies [3–10]. Interest in this field has been motivated by the desire for a better fundamental understanding of the nonlinear dynamics of these supersonic combustion waves, and more recently, by some promising applications such as rotating detonation engines [11–16], in which the instability of detonations has a major impact on the system performance.

Since the 1990s, significant advances toward the understanding of the strongly nonlinear dynamics of detonation fronts have been made by theoretical analyses (see [17,18] and references therein). However, very few asymptotic analyses providing constitutive models describing the behavior of these unsteady supersonic combustion waves have been reported in the literature. Indeed, the unsteady coupling between the shock discontinuity and the combustion chemistry controlling the amount of heat release makes addressing the problem through analytical developments a quite challenging task. The most recent progress in this direction concerns the direct initiation of gaseous detonations for which theoretical analyses have been completed with success [19,20]. Such asymptotic analyses are built after carefully calibrating control parameters, with the ultimate objective of improving our understanding by retaining the key mechanisms at the expense of others, which are expected to be less influential. The purpose is thus to simplify the formulation in a systematic way for obtaining analytical solutions, which then describe the main features of the phenomena at play.

The present work revisits previous asymptotic developments [21] tackling the linear dynamics of weakly overdriven waves in the limit of small heat release and for a ratio of specific heats close to unity, i.e., the so-called Newtonian approximation. Weakly unstable waves in the Chapman-Jouguet (CJ) regime are considered in the current work (cf. Fig. 1), and three major simplifications arise in the asymptotic analysis: firstly, compressional heating within the inner structure of the detonation is shown to be negligible in comparison to heating by combustion, which is a rather valid approximation for a generic gaseous detonation. Secondly, in association with the limit of small heat release, the variation of the speed of sound with temperature is negligible. Thirdly, a two-timescale dynamics is shown to control the response of heat release in the reaction zone to velocity fluctuations of the leading shock. The two time scales are associated to disturbances developing within the detonation and propagating upstream and downstream respectively, as illustrated in Fig. 1. Due to the transonic nature of the flow (within the inner structure

* Corresponding author.
E-mail address: luc.vervisch@insa-rouen.fr (L. Vervisch).

https://doi.org/10.1016/j.combustflame.2021.111535
0010-2180/

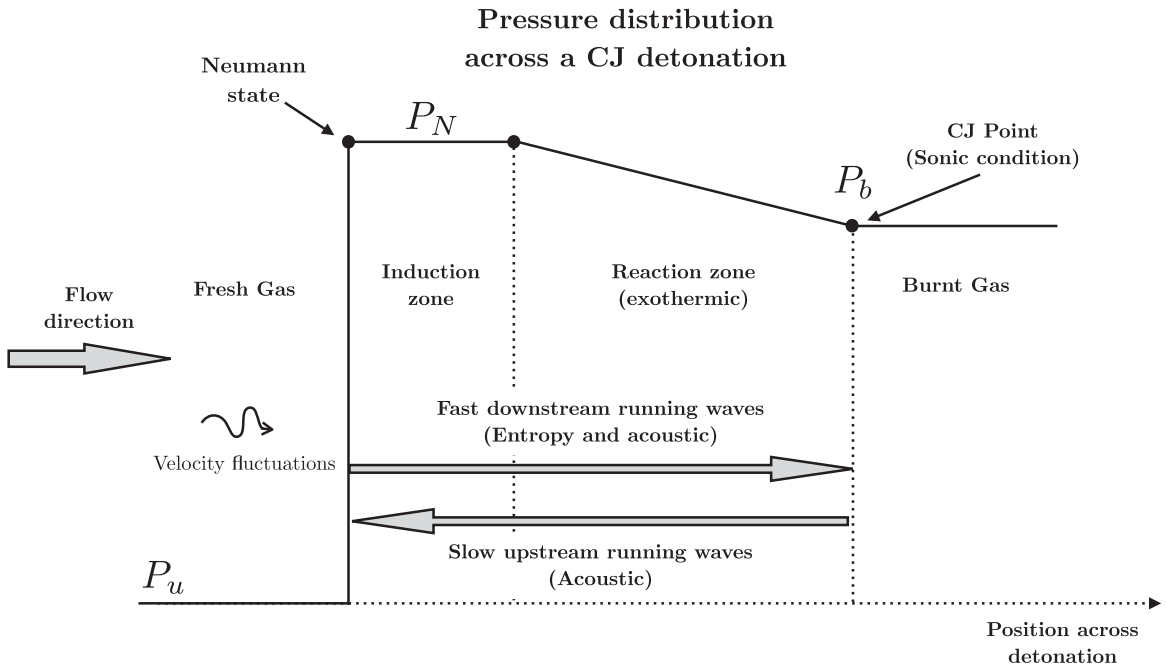

Fig. 1. Schematic representation of the pressure distribution across a Chapman-Jouguet detonation with characteristics instability modes.

of the detonation) in the double limit of small heat release and unity ratio of specific heats, the disturbances propagating via the downstream modes can be considered to be quasi-instantaneous, and the dynamics of the unsteady detonation is only controlled by the upstream-running mode.

In the Chapman-Jouguet regime of real detonations (i.e. outside the asymptotic limits considered for the study), the flow relative to the lead shock is sonic at the end of the reaction zone, but is substantially subsonic at the Neumann state, so that the two-timescale nature of the dynamics is less pronounced. Even though the absolute values of the parameters characterizing the dynamics of these real detonations can be quantitatively different, the general trends reported in this study remain nonetheless qualitatively valid. Specifically, the role of the characteristics loops between the lead shock and the reaction zone (as summarized in Fig. 1), appears as the driving mechanism of detonation instability. This coupling mechanism remains equally relevant for realistic detonations, although the two time-scale nature of the characteristic waves is less pronounced for detonations observed in real systems.

In the theoretical part of the current work, the time-dependent velocity of the lead shock is obtained as an eigenfunction of a single hyperbolic equation for the flow velocity with two boundary conditions, one at the Neumann state using the Rankine-Hugoniot conditions, and the other in the burnt gas where a sonic condition is applied for the CJ regime. The flow is fed by an unsteady reaction rate whose time dependence is through the shock velocity only. The solution is then cast in the form of an integral equation for the time-dependent shock velocity of a weakly unstable detonation, just above the instability threshold. In this analysis, combustion chemistry appears only through the distribution of the heat release rate, with the chemical time scale introduced as a free parameter.

Theoretical results are validated against direct numerical simulations. In the numerical study, the one-dimensional reactive Euler equations are solved using the high-order spectral difference (SD) method [22–24]. Numerical simulations resolving the oscillations in time are performed in the double limit of low heat release and specific heat ratios close to unity. A modified single-step Arrhenius chemistry whose time dependence follows a scaling law approximating heat-release profiles for real hydrogen-oxygen detonations [25] is used. A recently proposed shock capturing approach for high-order methods based on characteristic waves is applied [26] in order to minimize post-shock numerical aberrations.

The paper is organized as follows: the flow configuration under study and the theoretical formulation are presented in the subsequent section. Then, the asymptotic analysis leading to an integral equation for the shock velocity of the CJ detonation is presented. The specific framework of the parametric analysis for the comparison of numerical and theoretical results is then discussed. After that, the numerical analysis is presented and results are compared against the theoretical predictions, before concluding.

2. Flow configuration and theoretical formulation

2.1. Primitive balance equations

In a planar geometry, Euler's equations of a reactive gas flow take the form

$$\frac{1}{\rho}\left(\frac{\partial}{\partial t}+u\frac{\partial}{\partial x}\right)\rho+\frac{\partial u}{\partial x}=0,$$
$$\rho\left(\frac{\partial}{\partial t}+u\frac{\partial}{\partial x}\right)u=-\frac{\partial p}{\partial x}, \tag{1}$$

$$\left(\frac{\partial}{\partial t}+u\frac{\partial}{\partial x}\right)\left[\ln T-\frac{(\gamma-1)}{\gamma}\ln p\right]=\frac{q_m}{c_pT}\frac{w(T,Y)}{t_r},$$
$$\left(\frac{\partial}{\partial t}+u\frac{\partial}{\partial x}\right)Y=\frac{w(T,Y)}{t_r}, \tag{2}$$

where ρ is the density, p is the pressure, u is the flow velocity in the laboratory frame, $\gamma=c_p/c_v$ is the constant ratio of specific heat, q_m denotes the chemical heat release per unit mass of the mixture, T is the temperature, Y is the progress variable ($Y=0$ in the initial mixture and $Y=1$ in the burned gas, $1-Y$ is the reduced mass fraction of the limiting component in a one-step reac-

tion), t_r is the reaction time at the Neumann state of the planar CJ detonation and w denotes the non-dimensional heat-release rate.

Assuming the ideal gas law, the pressure p and the sound speed a may be written

$$p = \frac{\gamma - 1}{\gamma} c_p \rho T, \qquad a = \sqrt{\gamma \frac{p}{\rho}}. \tag{3}$$

Attention is focused on an irreversible exothermic reaction, whose rate

$$\dot{W}(T, Y) = \frac{w(T, Y)}{t_r} \geqslant 0 \tag{4}$$

depends on the temperature T and the mass fraction of the species Y, the pressure dependence of the reaction rate being neglected for simplicity in comparison to the thermal sensitivity.

Boundary conditions may be applied at the compressed side of the lead shock and at the exit of the reaction zone. Let us consider a propagation from right to left with an orientation of the axis towards the burnt gas, the gas flowing in the negative direction $u < 0$ in the laboratory frame. The lead shock of the detonation is modelled as a discontinuity in the flow of inert gas at initial temperature T_u (composition of frozen fresh gases $Y = Y_u$, $w(T_u, Y_u) = 0$). The boundary conditions on the shock (the Neumann state is denoted by the subscript N) are given by the Rankine-Hugoniot jump relations

$$Y_N = Y_u, \quad \frac{p_N}{p_u} = 1 + \frac{2\gamma}{\gamma + 1}(M^2 - 1), \quad \frac{\rho_N}{\rho_u} = \frac{1 + (M^2 - 1)}{1 + \frac{\gamma - 1}{\gamma + 1}(M^2 - 1)},$$
$$\frac{u_N}{a_u} = -\left(1 - \frac{\rho_u}{\rho_N}\right) M, \tag{5}$$

where the subscript u denotes the fresh mixture at rest and $M \equiv \mathcal{D}/a_u > 1$ is the propagation Mach number, $\mathcal{D}$ being the propagation velocity of the lead shock. For a weak shock $0 < M - 1 \ll 1$, the system of Eq. (5) reads

$$\frac{T_N}{T_u} = 1 + 4\frac{(\gamma - 1)}{\gamma + 1}(M - 1) + \mathcal{O}\left[(M - 1)^2\right], \tag{6}$$

$$\frac{p_N}{p_u} = 1 + 4\frac{\gamma}{\gamma + 1}(M - 1) + \mathcal{O}\left[(M - 1)^2\right], \tag{7}$$

$$\frac{u_N}{a_u} = -\frac{4}{\gamma + 1}(M - 1) + \frac{2}{\gamma + 1}(M - 1)^2 + \mathcal{O}\left[(M - 1)^3\right], \tag{8}$$

$$\frac{U_N}{a_u} \equiv \frac{u_N}{a_u} + M = 1 - \frac{3 - \gamma}{\gamma + 1}(M - 1) + \frac{2}{\gamma + 1}(M - 1)^2 + \mathcal{O}\left[(M - 1)^3\right]. \tag{9}$$

Considering a CJ detonation propagating in an infinite medium, the boundary condition at the exit of the reaction zone is a sonic condition, meaning that compressible waves in the flow of burnt gas cannot enter the reaction zone (i.e., radiation condition).

2.2. Characteristic equations in the moving frame

An alternative form of the energy equation in (2) is expressed in terms of p and u, by using the ideal gas law (3) when ρ is eliminated from the mass conservation equation in (1),

$$\frac{1}{\gamma p}\left(\frac{\partial}{\partial t} + u\frac{\partial}{\partial x}\right) p + \frac{\partial u}{\partial x} = \frac{q_m}{c_p T}\frac{w(T, Y)}{t_r}. \tag{10}$$

The equations for the conservation of mass and momentum in (1) can be put in the form of two hyperbolic equations for u and p when the equation for conservation of momentum in (1) is multiplied by $a/(\gamma p) = 1/(\rho a)$, then added to and subtracted from (10):

$$\frac{1}{\gamma p}\left[\frac{\partial}{\partial t} + (u \pm a)\frac{\partial}{\partial x}\right] p \pm \frac{1}{a}\left[\frac{\partial}{\partial t} + (u \pm a)\frac{\partial}{\partial x}\right] u = \frac{q_m}{c_p T}\frac{w(T, Y)}{t_r}. \tag{11}$$

These equations, relating the propagation of the disturbances of pressure p and flow velocity u to the rate of heat release w/t_r, are the simple extension of the usual characteristic equations (simple waves) to reacting gases. When (3) is used and when the chemical kinetics $w(T, Y)/t_r$ is known, the four equations in (2) and (11) form a closed set of equations for p, u, T and Y.

Considering the intrinsic dynamics of a Chapman-Jouguet wave, the flow in the burnt gas $u = u_b$, $p = p_b$, $w = 0$, the sonic condition for the unperturbed wave propagating at the constant CJ velocity $\overline{\mathcal{D}}$ and the radiation condition yield

$$\overline{\mathcal{D}} + \overline{u}_b = \overline{a}_b, \qquad \delta p_b + \overline{\rho}_b \overline{a}_b \delta u_b = 0, \tag{12}$$

where the overline denotes the unperturbed solution, and the decomposition $z = \overline{z} + \delta z$ has been used.

The equation for the trajectory of the shock front in the laboratory frame,

$$x = x_f(t), \quad \mathrm{d}x_f/\mathrm{d}t = -\mathcal{D}(t) < 0, \quad u < 0, \tag{13}$$

suggests that it is convenient to use the reference frame attached to the lead shock:

$$\mathrm{x} \equiv x - x_f(t) \quad \Rightarrow \quad \partial/\partial x \to \partial/\partial \mathrm{x}, \quad \partial/\partial t \to \partial/\partial t + \mathcal{D}(t)\partial/\partial \mathrm{x}, \tag{14}$$

$\mathcal{D} + u > 0$ being the flow velocity relative to the shock. The boundary conditions at the Neumann state take the form

$$\mathrm{x} = 0: \quad Y = Y_u, \quad p = p_N(t), \quad T = T_N(t), \quad u = u_N(t) < 0, \tag{15}$$

where $p_N(t)$, $T_N(t)$, and $u_N(t)$ are given in term of the instantaneous propagation velocity $\mathcal{D}(t)$ in (5). Introducing the non-dimensional coordinate ξ, attached to the moving front of the lead shock and reduced by the thickness of the unperturbed CJ detonation (denoted by an over-bar),

$$\xi \equiv \frac{x - x_f(t)}{\overline{U}_N t_r}, \quad \text{with} \quad \overline{U}_N \equiv \overline{\mathcal{D}} + \overline{u}_N, \quad 0 < \overline{U}_N < \overline{a}_N, \tag{16}$$

Eqs. (2) and (11) become

$$\left[t_r\frac{\partial}{\partial t} + \frac{(u + \mathcal{D})}{\overline{U}_N}\frac{\partial}{\partial \xi}\right]\left[\ln T - \frac{(\gamma - 1)}{\gamma}\ln p\right] = \frac{q_m}{c_p T} w(T, Y),$$
$$\left[t_r\frac{\partial}{\partial t} + \frac{(u + \mathcal{D})}{\overline{U}_N}\frac{\partial}{\partial \xi}\right] Y = -w(T, Y), \tag{17}$$

$$\left[t_r\frac{\partial}{\partial t} + \frac{(\mathcal{D} + u \pm a)}{\overline{U}_N}\frac{\partial}{\partial \xi}\right]\ln p \pm \gamma\frac{a_u}{a}\left[t_r\frac{\partial}{\partial t} + \frac{(\mathcal{D} + u \pm a)}{\overline{U}_N}\frac{\partial}{\partial \xi}\right]\frac{u}{a_u} = \gamma\frac{q_m}{c_p T} w(T, Y). \tag{18}$$

The boundary conditions (12) and (15) have to be used at $\xi \to \infty$ and $\xi = 0$, respectively.

3. Asymptotic analysis

In this section, we revisit the linear analysis [21] in the limit of small heat release, with a particular attention to the Chapman-Jouguet wave and to the weakly nonlinear solutions just above the instability threshold.

3.1. Asymptotic limit and the two-timescale dynamics

The analysis is performed in the limit of small heat release $\mathcal{Q} \equiv [(\gamma+1)/2]q_m/c_pT_u \ll 1$ by introducing the small parameter ϵ and using the following distinguished limit:

$$\epsilon \equiv \sqrt{\mathcal{Q}} \ll 1, \qquad (\gamma-1)/\epsilon \ll 1. \tag{19}$$

The propagation Mach number of the planar CJ wave $\overline{M} = \sqrt{\mathcal{Q}} + \sqrt{\mathcal{Q}+1}$ differs from unity by a small amount $\overline{M} - 1 = \epsilon + \mathcal{O}(\epsilon^2)$. For $\overline{M} - 1 \ll 1$, the lead shock is weak. Yet, it can be considered as a discontinuity in a flow governed by the Euler equations if the reaction rate $1/t_r$ is much smaller than the elastic collision rate $1/t_c$ and if the detonation thickness $a_u t_r$ is much larger than the thickness of the lead shock $a_u t_c/(M-1)$ [18]. This is still the case in the asymptotic limit $\epsilon \to 0$, provided that the following ordering is satisfied: $t_r/t_c \gg 1/\epsilon$. Notice, however, that the entropy jump across the lead shock is negligible [18].

In the limit (19), the Rankine-Hugoniot conditions (5) read,

$$\frac{\overline{p}_N}{p_u} - 1 = 2\epsilon + \mathcal{O}(\epsilon^2), \qquad \frac{\overline{T}_N}{T_u} - 1 = \mathcal{O}[(\gamma-1)\epsilon],$$
$$\frac{a_u}{\overline{U}_N} = 1 + \mathcal{O}(\epsilon), \tag{20}$$

$$\frac{\overline{D} - a_u}{a_u} = \epsilon + \mathcal{O}(\epsilon^2), \quad \frac{\overline{u}_N + \overline{\mathcal{D}} - a_u}{\overline{U}_N} = -\epsilon + \mathcal{O}(\epsilon^2),$$
$$\frac{\overline{u}_N + \overline{\mathcal{D}} + a_u}{\overline{U}_N} = 2 - \epsilon + \mathcal{O}(\epsilon^2). \tag{21}$$

The attention is now focussed on disturbances that are of the same order of magnitude as $(\overline{\mathcal{D}} - a_u)/a_u = \mathcal{O}(\epsilon)$ but, as we shall see, with a thermal sensitivity of the reaction rate sufficiently large to have variations which are of the order of unity. The non-dimensional flow velocity and the shock velocity, respectively, μ and $\dot{\alpha}_\tau$, both of them of order unity, are introduced in the limit (19)

$$\epsilon \to 0: \qquad \mu = \mathcal{O}(1), \qquad \dot{\alpha}_\tau = \mathcal{O}(1), \tag{22}$$

$$\frac{\overline{\mathcal{D}} + u}{a_u} \equiv 1 - \epsilon\mu, \quad \frac{\mathcal{D} - \overline{\mathcal{D}}}{a_u} \equiv \epsilon\dot{\alpha}_\tau$$
$$\Rightarrow \frac{\mathcal{D} + u}{a_u} = 1 - \epsilon(\mu - \dot{\alpha}_\tau), \; M - 1 = \epsilon + \epsilon\dot{\alpha}_\tau + \mathcal{O}(\epsilon^2), \tag{23}$$

$$\frac{a}{a_u} = 1 + \mathcal{O}(\epsilon^2) \Rightarrow \frac{\mathcal{D} + u + a}{a_u} = 2 + \mathcal{O}(\epsilon),$$
$$\frac{\mathcal{D} + u - a}{a_u} = -\epsilon(\mu - \dot{\alpha}_\tau) + \mathcal{O}(\epsilon^2), \tag{24}$$

where the first relation in (24) comes from $q_m/c_pT_u = \mathcal{O}(\epsilon^2) \Rightarrow (T - T_N)/T_N = \mathcal{O}(\epsilon^2)$.

According to the last equation in (20), the sound speed a_u in the denominator of the two last relations in (24) can be replaced by $\overline{U}_N$ without modification of the leading order, showing the quasi-transonic character of the flow $u + \mathcal{D}$ in the frame attached to the lead shock. According to (7), (9) and (23), the Rankine-Hugoniot conditions at the Neumann state take the form

$$\xi = 0: \; p = p_N, \; T = T_N, \; \mu = \mu_N;$$
$$p_N/p_u = 1 + 2\epsilon(1 + \dot{\alpha}_\tau) + \mathcal{O}(\epsilon^2), \tag{25}$$

$$T_N/T_u = 1 + 2(\gamma-1)[1 + \epsilon(1 + \dot{\alpha}_\tau) + \mathcal{O}(\epsilon^2)], \tag{26}$$

$$\mu_N = 1 + 2\dot{\alpha}_\tau + \mathcal{O}(\epsilon), \tag{27}$$

and, the boundary condition in the burnt gas (12) yields

$$\xi \to \infty: \quad w = 0, \quad \overline{\mu} = 0 \quad \text{(sonic condition)}, \tag{28}$$

but no condition on $\delta\mu$ is prescribed in the burnt gas to leading order in the limit $\epsilon \to 0$, since, according to the definition of μ in (23), $\epsilon\delta\mu_b = -\delta u_b/\overline{a}_b$, which simply implies the order of magnitude of δu_b, namely, $\delta u_b/\overline{a}_b = \mathcal{O}(\epsilon)$. In relation with (25), it is convenient to introduce the reduced pressure, of order unity in the limit $\epsilon \to 0$,

$$p/\overline{p}_N - 1 \equiv \epsilon\pi, \quad \pi = \mathcal{O}(1); \qquad \xi = 0: \quad \pi = \pi_N;$$
$$\pi_N = 2\dot{\alpha}_\tau + \mathcal{O}(\epsilon). \tag{29}$$

According to (24), Eq. (18) exhibit the two-timescale nature of the compressible waves; the upstream-running one (propagating toward the lead shock) has a velocity smaller than the velocity of the downstream running one by a factor ϵ. Eq. (17) is the downstream-running entropy wave which is convected by the flow $u + \mathcal{D}$. The dynamics is resulting from a continuous set of loops constituted by two downstream-running modes and an upstream-running one. Disturbances are generated at the shock by the fluctuations of the propagation velocity $\mathcal{D}(t)$. They are propagated through the detonation thickness by the downstream-running modes, perturbing the distribution of the reaction rate. Disturbances are then sent back to the lead shock by the upstream-running mode, closing the loop.

An instability develops if the retroaction on the shock velocity, delayed by the loops, is in phase with the emission. In the limit $\epsilon \to 0$, the downstream running modes are infinitely faster than the upstream-running one and they produce quasi-instantaneous disturbances. The dynamics of the lead shock is controlled by the upstream-running mode (the slowest in the loop) and, according to (16) and the second equation in (24), the characteristic time of evolution is longer than the transit time t_r of a fluid particle across the inner structure of the detonation by a factor of order ϵ. It is therefore useful to introduce the time of order unity $\tau = \mathcal{O}(1)$

$$\tau \equiv \epsilon\frac{t}{t_r} = \mathcal{O}(1), \qquad \frac{\partial}{\partial t} = \frac{\epsilon}{t_r}\frac{\partial}{\partial \tau}. \tag{30}$$

3.2. Unsteady distribution of heat release and scaling law

The differential operator on the left-hand side of Eq. (17) takes the form

$$\epsilon\partial/\partial\tau + [1 + \mathcal{O}(\epsilon)]\partial/\partial\xi \approx \partial/\partial\xi,$$

so that, to leading order in the limit $\epsilon \to 0$, the equations of species and energy are in steady state.

Neglecting corrections of order smaller than ϵ^2, the approximation $q_m/c_pT_u \approx \epsilon^2$ can be applied to Eqs. (17) and (18), showing that the relative variation of the energy is of order ϵ^2. After dividing by ϵ^2, the reduced energy on the left-hand side of the first equation in (17), $(T - \overline{T}_N)/(\epsilon^2\overline{T}_N) + [(\gamma-1)/(\epsilon\gamma)]\pi$, varies in the order of unity and, to leading order in the limit (19), $(\gamma-1)/\epsilon \ll 1$, compressional heating is negligible.

To leading order, the equations for conservation of species and energy reduce to

$$\frac{1}{\epsilon^2\overline{T}_N}\frac{\partial T}{\partial \xi} = \frac{\partial Y}{\partial \xi} = w(T, Y), \tag{31}$$

$$\xi = 0: \; T = T_N(\tau), \quad Y = 0; \qquad \xi = \xi_b \to \infty: \; Y = 1,$$
$$w(T, 1) = 0, \tag{32}$$

where Y has been considered here as the progress variable for simplicity. The final result is more general and can be applied to any distribution of heat released by combustion. The asymptotic

limit $\epsilon \to 0$ of (31) and (32) is meaningful only for small fluctuations of the Neumann temperature $(T_N(\tau) - \overline{T}_N)/(\epsilon \overline{T}_N) = \mathcal{O}(\epsilon^2)$, so that the reduced temperature of order unity in (31) is $\theta \equiv (T - \overline{T}_N)/(\epsilon^2 \overline{T}_N)$. The time dependence of the detonation structure is through the Neumann temperature $T_N(\tau)$ only and the instantaneous distribution of the unsteady heat release $w_o[\xi, T_N(\tau)]$ is obtained by solving the steady-state problem (31) and (32), with $\int_0^\infty w_o(\xi, T_N) \mathrm{d}\xi = 1$. According to (26), $(T_N - \overline{T}_N)/\overline{T}_N = 2(\gamma - 1)\epsilon \dot{\alpha}_\tau$, the thermal sensitivity of $w(T, Y)$ should be strong enough to produce a non trivial effect in the limit $\epsilon \to 0$.

For simplicity, we will use a scaling law for the unsteady distribution of reaction rate. The chemical kinetics of ordinary combustible mixtures is constituted by initiation steps, chain-branching steps and recombination reactions. The corresponding spatial distribution of heat release rate in a detonation wave is constituted by an induction zone, followed by a zone of heat release. The thermal sensitivity of the induction length is described by an Arrhenius law, $l_{ind}(T_N) \propto a_u t_r \mathrm{e}^{E/(k_b T_N)}$, where E is the activation energy of the chain-branching step [18],

$$l_{ind}(T_N)/l_{ind}(\overline{T}_N) = \exp\left[\frac{E}{k_B \overline{T}_N}\left(\frac{\overline{T}_N}{T_N} - 1\right)\right], \quad \text{with}$$
$$\overline{T}_N/T_N - 1 = -2(\gamma - 1)[\epsilon \dot{\alpha}_\tau + \mathcal{O}(\epsilon^2)], \tag{33}$$

where (26) has been used. Introducing the reduced activation energy b of order unity, the induction length is expressed in terms of the propagation velocity $\dot{\alpha}_\tau(\tau)$ in the form

$$b \equiv 2(E/k_B \overline{T}_N)(\gamma - 1)\epsilon = \mathcal{O}(1), \qquad l_{ind}(T_N)/l_{ind}(\overline{T}_N) = \mathrm{e}^{-b\dot{\alpha}_\tau(\tau)}. \tag{34}$$

Assuming that the strongest temperature dependence of the reaction rate comes from the induction reactions and neglecting all the other temperature dependence in the limit $\epsilon \to 0$, the unsteady distribution of heat release is approximated by a scaling law,

$$w_o^{(sl)}[\xi, T_N(\tau)] = \frac{l_{ind}(\overline{T}_N)}{l_{ind}(T_N)} \overline{w}_o\left[\frac{x - x_f(\tau)}{l_{ind}(T_N)}\right] = \mathrm{e}^{b\dot{\alpha}_\tau(\tau)} \overline{w}_o\left[\xi \mathrm{e}^{b\dot{\alpha}_\tau(\tau)}\right], \tag{35}$$

where $\overline{w}_o(\xi)$, $\int_0^\infty \overline{w}_o(\xi)\mathrm{d}\xi = 1$, is the normalized distribution of the unperturbed CJ wave, the reference time t_r used in Eq. (16) being defined as $\overline{U}_N t_r = l_{ind}(\overline{T}_N)$. It turns out that the approximation (35) is satisfactory for hydrogen flames, see Fig. 2 in [25]. For a better quantitative accuracy, the distribution $w_o[\xi, T_N(\tau)]$, solution of the steady equations of energy and species in (31) and (32), could be used. From now on we will use the notation

$$y(\tau) \equiv b\dot{\alpha}_\tau(\tau) = O(1) \quad \text{and write}$$
$$w_o^{(sl)}[\xi, T_N(\tau)] = \mathrm{e}^{y(\tau)} \overline{w}_o[\xi \mathrm{e}^{y(\tau)}]. \tag{36}$$

3.3. Integral equation

Using (23) and (24) and (29)–(30), Eq. (18) divided by ϵ^2 yield

$$\left\{\frac{\partial}{\partial \tau} + \left[\frac{2}{\epsilon} + \mathcal{O}(1)\right]\frac{\partial}{\partial \xi}\right\}(\pi - \mu) = w_o[\xi, y(\tau)], \tag{37}$$

$$\left\{\frac{\partial}{\partial \tau} - [(\mu - y/b) + \mathcal{O}(\epsilon)]\frac{\partial}{\partial \xi}\right\}(\pi + \mu) = w_o[\xi, y(\tau)], \tag{38}$$

where we have used the more transparent notation $w_o[\xi, y(\tau)]$ in place of $w_o[\xi, T_N(\tau)]$. To leading order in the limit $\epsilon \to 0$, Eq. (37) shows that

$$\frac{\partial}{\partial \xi}(\pi - \mu) = 0. \tag{39}$$

In addition, from Eqs. (27) and (29) we get

$$\mu_N = 1 + \pi_N. \tag{40}$$

Eqs. (39) and (40) then imply that

$$\pi(\xi, \tau) = \mu(\xi, \tau) - 1. \tag{41}$$

Substituting the above equation into (38), the problem reduces to solving a single hyperbolic equation for the flow $\mu(\xi, \tau)$, fed by the heat release $w_o[\xi, y(\tau)]$:

$$\frac{\partial \mu}{\partial \tau} - \left[\mu - \frac{y(\tau)}{b}\right]\frac{\partial \mu}{\partial \xi} = \frac{1}{2} w_o[\xi, y(\tau)], \tag{42}$$

which is the simple wave corresponding to the upstream-running mode (propagating in the negative direction, i.e. from the reacting gas to the lead shock). The boundary conditions are (12) at infinity and (27) at $\xi = 0$. The flow of the unperturbed CJ detonation ($\overline{y} = 0$) is $\overline{\mu}(\xi) \in [0, 1]$,

$$\overline{\mu}(\xi) = \sqrt{1 - \int_0^\xi \overline{w}_o(\xi')\mathrm{d}\xi'}, \quad \int_0^\infty \overline{w}_o(\xi')\mathrm{d}\xi' = 1,$$
$$\overline{w}_o(\xi) = w_o(\xi, y = 0) > 0. \tag{43}$$

The time-dependent propagation velocity $y(\tau)$ (with $\overline{y} = 0$) is obtained as an eigenfunction of the problem (42) with, according to (27)–(28), the following boundary conditions for the solution $\mu(\xi, \tau)$:

$$\xi = 0: \ \mu = 1 + 2y(\tau)/b,$$
$$\xi \to \infty: \ \overline{\mu} = 0, \ \mu = \delta\mu_b \quad \text{where } \delta\mu_b \text{ is not known}, \tag{44}$$

see the text below (28). It turns out that the linear solution of (42)–(44) is obtained without any requirement concerning $\delta\mu_b$. Linearization of the flow field $\mu = \overline{\mu}(\xi) + \delta\mu(\xi, \tau)$ on the left-hand side of (42) yields

$$\frac{\partial}{\partial \tau}\delta\mu - \frac{\partial}{\partial \xi}(\overline{\mu}\delta\mu) = \mathcal{G}[\xi, y(\tau)],$$
$$\mathcal{G}[\xi, y(\tau)] \equiv \frac{1}{2}\{w_o[\xi, y(\tau)] - \overline{w}_o(\xi)\} - \frac{1}{b}\frac{\mathrm{d}\overline{\mu}}{\mathrm{d}\xi} y, \tag{45}$$

$$\frac{\partial}{\partial \tau}(\overline{\mu}\delta\mu) - \overline{\mu}(\xi)\frac{\partial}{\partial \xi}(\overline{\mu}\delta\mu) = \overline{\mu}(\xi)\mathcal{G}[\xi, y(\tau)]. \tag{46}$$

It is useful to introduce the change of variable $\zeta(\xi) \in [0, \infty)$:

$$\zeta(\xi) = \int_0^\xi \frac{\mathrm{d}\xi'}{\overline{\mu}(\xi')}, \qquad \overline{\mu}(\xi)\frac{\partial}{\partial \xi} = \frac{\partial}{\partial \zeta}, \tag{47}$$

which is a one-to-one correspondence between ξ and ζ inside the inner structure, since the function $\overline{\mu}(\xi)$ remains positive (it decreases monotonically from 1, at $\xi = 0$, to 0, for $\xi \to \infty$). Introducing the new functions $F(\zeta, \tau)$ and $Z(\zeta, \tau)$,

$$F(\zeta, \tau) \equiv \overline{\mu}[\xi(\zeta)]\mathcal{G}[\xi(\zeta), y(\tau)],$$
$$Z(\zeta, \tau) \equiv \overline{\mu}[\xi(\zeta)]\delta\mu[\xi(\zeta), \tau], \tag{48}$$

Eq. (46) and the boundary conditions (44) become:

$$\frac{\partial Z}{\partial \tau} - \frac{\partial Z}{\partial \zeta} = F(\zeta, \tau), \quad \zeta = 0: \ Z = 2y(\tau)/b, \quad \zeta \to \infty: \ Z \to 0, \tag{49}$$

where the boundary condition at infinity comes from the limits $\lim_{\xi \to \infty} \zeta(\xi) = \infty$ and $\lim_{\xi \to \infty} \overline{\mu}(\xi) = 0$ and one has $\lim_{\zeta \to \infty} F(\zeta, \tau) = 0$.

The general solution of the hyperbolic Eq. (49) is

$$Z(\zeta, \tau) - Z(0, \tau + \zeta) = -\int_0^\zeta F(\zeta', \zeta + \tau - \zeta')\mathrm{d}\zeta'. \tag{50}$$

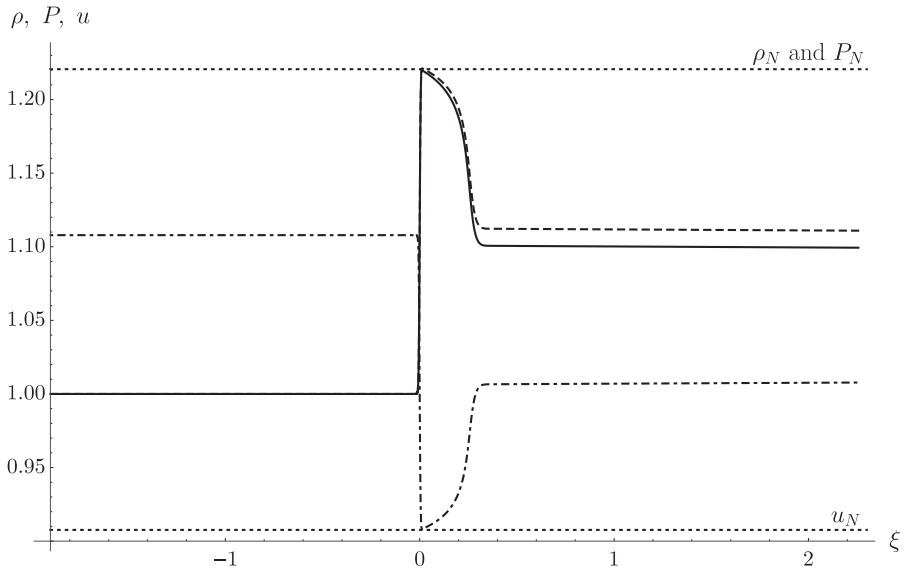

(a) Full domain

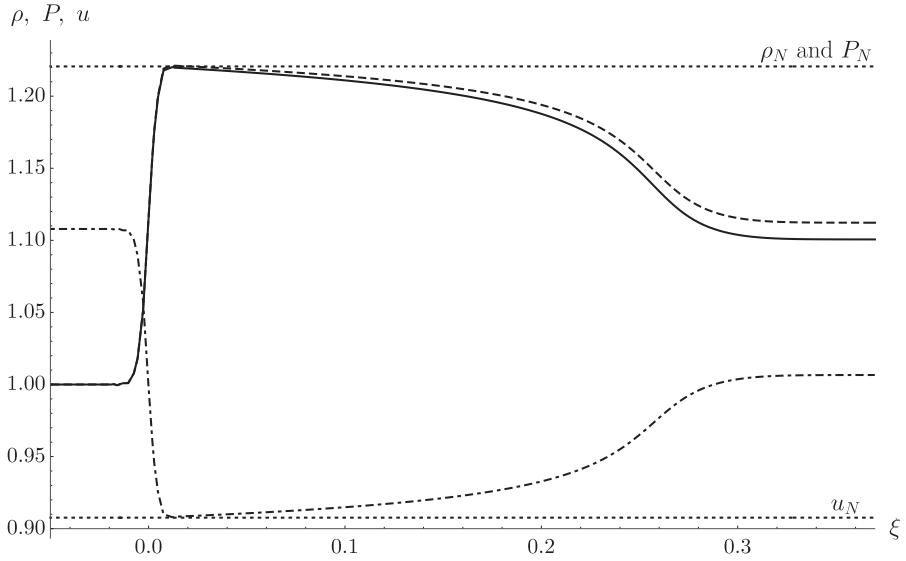

(b) Zoom into the detonation

Fig. 2. Distributions across CJ steady detonation for $\gamma = 1.005$, $\epsilon = 0.1$, $\beta = 5$, $b = 0.9$: solid line, normalized density; dashed line, normalized pressure; dash-dotted line, normalized flow velocity; dotted line; Neumann conditions.

Hence, taking the limits $\zeta \to \infty$ and $\tau \to \infty$, keeping $\tau + \zeta$ constant and equal to τ_o, $\tau + \zeta = \tau_o$, the boundary condition $\lim_{\zeta\to\infty} Z(\zeta, \tau) \to 0 \ \forall \tau$ yields

$$Z(0, \tau_o) = \int_0^\infty F(\zeta', \tau_o - \zeta')\mathrm{d}\zeta', \tag{51}$$

which, when using the boundary condition at the Neumann state in (49), $\zeta = 0 :\ Z = 2y(\tau)/b$, becomes an integral equation of the form

$$2y(\tau) = b\int_0^\infty F(\zeta, \tau - \zeta)\mathrm{d}\zeta, \tag{52}$$

in which the subscript of τ_o has been suppressed.

According to (45) and (48), the time dependence of $F(\zeta, \tau)$ is through $y(\tau)$, so that Eq. (52) is an integral equation for the velocity of the lead shock, $y(\tau) \equiv b\dot{\alpha}_\tau(\tau)$, involving an integration on the time delay associated with the transit time of the upstream-propagating mode, from each point inside the inner-detonation-structure to the lead shock (continuous set of loops mentioned at the end of Section 3.1).

3.4. Instability threshold for the scaling law

When considering the stability limit, the function $F(\zeta, \tau)$ has to be linearized. Using the scaling law (35), the linearization yields

$$b\delta F(\zeta, \tau) = g(\zeta)y(\tau), \qquad g(\zeta) \equiv \overline{\mu}[\xi(\zeta)]G[\xi(\zeta)],$$
$$G(\xi) \equiv \frac{\mathrm{d}}{\mathrm{d}\xi}\left[\frac{b}{2}\xi\overline{w}_o(\xi) - \overline{\mu}(\xi)\right], \tag{53}$$

so that, according to (52), the linear integral relation for the propagation velocity takes the form

$$2y(\tau) = \int_0^\infty g(\zeta)y(\tau-\zeta)\mathrm{d}\zeta. \tag{54}$$

Using a normal mode analysis, $y(\tau) \propto \mathrm{e}^{\sigma\tau}$, a transcendental equation is obtained for the complex linear growth rate σ in the form of an equation for a Laplace transform

$$2 = \int_0^\infty g(\zeta)\mathrm{e}^{-\sigma\zeta}\mathrm{d}\zeta, \qquad 2 = \int_0^\infty G(\xi)\mathrm{e}^{-\sigma\int_0^\xi \mathrm{d}\xi'/\overline{\mu}(\xi')}\mathrm{d}\xi, \tag{55}$$

which is an equation similar to that obtained previously for weakly overdriven detonations [21].

Setting $\sigma = s + i\omega$, $s = \Re(\sigma)$, $\omega = \Im(\sigma)$, two equations are obtained for determining the oscillatory frequency and the critical value of b at the instability threshold ($s = 0$: $b = b^*$, $\omega = \omega^*$),

$$2 = \int_0^\infty g(\zeta)\cos(\omega\zeta)\mathrm{d}\zeta, \qquad 0 = \int_0^\infty g(\zeta)\sin(\omega\zeta)\mathrm{d}\zeta. \tag{56}$$

These relations are valid for any complex set of elementary chemical reactions controlling the combustion kinetics. The only chemical parameter is the distribution $\overline{w}_o(\xi)$ of heat release in the unperturbed CJ wave. The stiffer the distribution $\overline{w}_o(\xi)$ is, the more unstable the detonation is; as a result, the value of b^* gets smaller and the oscillatory frequency ω^* gets larger. Therefore, the analysis is limited to chemical kinetics for which the distribution of heat release $\overline{w}_o(\xi)$ is sufficiently smooth for ω^* to be of order unity, such as to satisfy the two-timescale analysis. More precisely, the asymptotic analysis fails as soon as the distribution $\overline{w}_o(\xi)$ becomes sufficiently stiff to generate a threshold frequency ω^* of order $2\pi/\epsilon$.

4. Framework for the parametric analysis

4.1. Model of reaction rate

To ease the parametric study using numerical simulations, we will use the following model of burning rate

$$\dot{W}(Y,T) = B(1-Y)\exp\left(-\frac{E}{k_B T_N}\right)\exp\left[\frac{E_T}{k_B T_N}\left(1-\frac{T_N}{T}\right)\right], \tag{57}$$

where B is the pre-exponential factor with the dimension of an inverse time. The reaction time at the Neumann state t_r is then given by

$$t_r = t_r(T_N) = \frac{1}{B}\exp\left(\frac{E}{k_B T_N}\right), \tag{58}$$

and $\dot{W}(Y,T)$ can be rewritten as

$$\dot{W}(Y,T) = \frac{w(Y,T)}{t_r} = \frac{1}{\bar{t}_r}(1-Y)\exp\left[\frac{-E}{k_B}\left(\frac{1}{T_N}-\frac{1}{\overline{T}_N}\right)\right] \times \exp\left[\frac{-E_T}{k_B}\left(\frac{1}{T}-\frac{1}{T_N}\right)\right], \tag{59}$$

where $\bar{t}_r = t_r(\overline{T}_N)$. This model, first introduced by Clavin and He [25], includes two activation energies: E, which governs the temperature sensitivity of the induction period, and E_T, which drives the temperature sensitivity of the rate of heat release. Typically, $E_T \ll E$ in order to clearly separate the induction zone from the reaction zone. The model aims to give a fair representation of the dynamics of real detonations, where small deviations in the temperature of the shocked gas T_N from the mean Neumann temperature $\overline{T}_N$, induce large variations in the rate of heat release.

However, for the model to be consistent with real detonations, the reaction rate should in addition stay negligible in the fresh gas. For this condition to be verified by Eq. (59) in the limit (19), the normalised activation energy $E_T/(k_B T_N)$ has to be too large, lying outside the range of interest in the current parametric study. Therefore, following the approach of Clavin and Williams [21], a cutoff temperature $T_c \in [T_u, T_N]$ is introduced so that the reaction rate is zero for temperatures below T_c, i.e.,

$$\dot{W}(Y,T) = \begin{cases} 0 & \text{for} \quad T \le T_c, \\ w(Y,T)/t_r & \text{for} \quad T > T_c, \end{cases} \tag{60}$$

where $w(Y,T)/t_r$ is given by (59).

4.2. Parameters formulation

First, it is observed that the burning rate in Eq. (59) may be recast in the form

$$\dot{W}(Y,T) = \frac{w(Y,T)}{t_r} = \frac{1}{\bar{t}_r}(1-Y)\exp\left[\frac{E-E_T}{k_B\overline{T}_N}\left(1-\frac{\overline{T}_N}{T_N}\right)\right] \times \exp\left[\frac{E_T}{k_B\overline{T}_N}\left(1-\frac{\overline{T}_N}{T}\right)\right]. \tag{61}$$

Then, the two reduced activation energies of order unity b and β are defined as

$$b \equiv 2(\gamma-1)\epsilon\frac{E-E_T}{k_B\overline{T}_N}, \qquad \beta \equiv \epsilon^2\frac{E_T}{k_B\overline{T}_N}. \tag{62}$$

Using the reduced propagation velocity of the lead shock $\dot{\alpha}_\tau(\tau)$ as given by Eq. (33), one obtains, for the reduced temperature of order unity,

$$\theta = \frac{T-T_N}{\epsilon^2\overline{T}_N} = \frac{T-\overline{T}_N}{\epsilon^2\overline{T}_N} - \frac{2(\gamma-1)\epsilon\dot{\alpha}_\tau(\tau)}{\epsilon^2\overline{T}_N} \approx \frac{T-\overline{T}_N}{\epsilon^2\overline{T}_N}. \tag{63}$$

Then, using the above expression for θ, along with the definitions of b, β and $\dot{\alpha}_\tau$, the reaction rate takes the form

$$w(Y,T) = \mathrm{e}^{b\dot{\alpha}_\tau(\tau)}(1-Y)\mathrm{e}^{\beta\theta}. \tag{64}$$

For steady Chapman-Jouguet waves, where, according to (23), $\dot{\alpha}_\tau(\tau) = (\mathcal{D}-\overline{\mathcal{D}})/(a_u\epsilon) = 0$, the burning rate is given by a set of profiles $\overline{w}_{o\beta}(\xi)$, all of them corresponding to the same propagation velocity $\overline{\mathcal{D}}$, whose stiffness increases with β. According to (31) and (32), these profiles are $\overline{w}_{o\beta}(\xi) = [1-\overline{Y}_\beta(\xi)]\mathrm{e}^{\beta\overline{\theta}_\beta(\xi)}$, where the functions $\overline{Y}_\beta(\xi) = \overline{\theta}_\beta(\xi)$ are solutions of

$$\frac{\mathrm{d}\overline{Y}_\beta}{\mathrm{d}\xi} = (1-\overline{Y}_\beta)\mathrm{e}^{\beta\overline{Y}_\beta}; \quad \xi = 0: \ \overline{Y}_\beta = 0,$$

$$\xi \to \infty: \ \overline{Y}_\beta = 1 \quad \text{and} \quad \overline{w}_{o\beta}(\xi) = \frac{\mathrm{d}\overline{Y}_\beta(\xi)}{\mathrm{d}\xi}. \tag{65}$$

Therefore, a parametric analysis of the dynamics is performed using the two scalars b and β. For every value of β there exists a threshold value b^* above which the detonation becomes unstable.

The function $y(\tau) = b\dot{\alpha}_\tau(\tau)$ is obtained from (52) using (43), (45), (48) and (65) with $w_o(\xi, y) \to w_{o\beta}(\xi, y)$ and $w_{o\beta}[\xi, y(\tau)] \equiv \mathrm{e}^{y(\tau)}\overline{w}_{o\beta}[\xi\mathrm{e}^{y(\tau)}]$, since the scaling law (35) is automatically satisfied for the reaction rate (60)–(64). The critical activation energy b^* and the corresponding oscillation frequency ω^* at the instability threshold are obtained from (53) to (56) for $\overline{w}_o(\xi) \to w_{o\beta}(\xi)$.

5. Numerical analysis

5.1. Problem formulation

After using asymptotic developments to anticipate the one-dimensional dynamics of gaseous detonations, the primitive equations are now solved numerically to assess the validity of the theoretical results. For that end, the one-dimensional Euler Eqs. (1) and (2) used above are cast in their conservative form

$$\frac{\partial \boldsymbol{U}}{\partial t} + \frac{\partial \boldsymbol{F}}{\partial x} = \boldsymbol{S}, \tag{66}$$

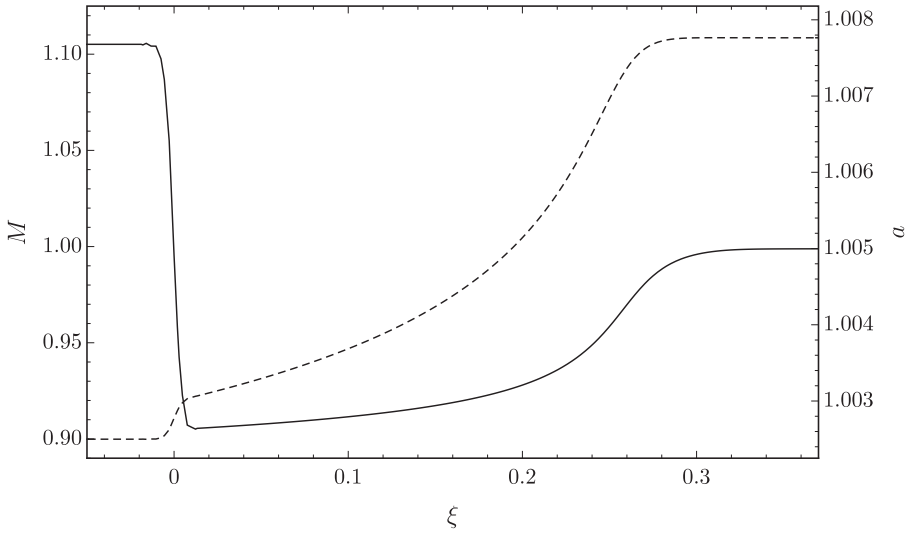

Fig. 3. Distributions across CJ steady detonation for $\gamma = 1.005$, $\epsilon = 0.1$, $\beta = 5$, $b = 0.9$: solid line, Mach number (left axis); dashed line, speed of sound (right axis).

where the vector of conservative variables **U**, the flux vector **F** and the source vector **S** are given respectively by

$$\mathbf{U} = \begin{pmatrix} \rho \\ \rho u \\ \rho E \\ \rho Y \end{pmatrix}, \quad \mathbf{F} = \begin{pmatrix} \rho u \\ \rho u^2 + p \\ \rho u E + p u \\ \rho u Y \end{pmatrix} \quad \text{and} \quad \mathbf{S} = \begin{pmatrix} 0 \\ 0 \\ \rho q_m \dot{W} \\ \rho \dot{W} \end{pmatrix}, \tag{67}$$

where E is the total energy (internal + kinetic) and $\dot{W}$ is given by Eq. (60). As previously, the system is closed with the equation of state (3).

For the numerical study, direct numerical simulations of one-dimensional CJ detonations are performed in the neighborhood of the double limit of small heat release and γ close to unity, Eq. (19). In practice, here $\gamma = 1.005$ and the normalized heat release per unit mass is set to $Q = (\gamma + 1) q_m / (2 c_p T_u) = 0.01 = \epsilon^2$. Then, as in the theoretical analysis, the numerical problem is fully characterized by the values of γ, ϵ, b, β and $\bar{t}_r$.

The numerical simulations are carried out in the reference frame of the steady CJ detonation, with the inlet flow velocity corresponding to the CJ Mach number [18]

$$\overline{M} = \sqrt{\mathcal{Q}} + \sqrt{\mathcal{Q} + 1}. \tag{68}$$

The outlet boundary condition corresponds to the sonic flow at the CJ state obtained via the Rankine-Hugoniot relations for a CJ detonation [3,18,27]:

$$\frac{p_b}{p_u} = \frac{\gamma \overline{M}^2 + 1}{\gamma + 1}, \tag{69}$$

$$\frac{\rho_b}{\rho_u} = \frac{(\gamma + 1)\overline{M}^2}{\gamma \overline{M}^2 + 1}, \tag{70}$$

$$\frac{u_b}{u_u} = \frac{\rho_u}{\rho_b}. \tag{71}$$

The computational domain extends along the streamwise direction for several times the detonation thickness, allowing the sonic condition to be well established at the outlet.

5.2. Numerical method

5.2.1. High-order spectral difference and shock capturing

All the details of the implementation of the numerical method are given in [26] and are not repeated here for sake of brevity, only the main lines are discussed.

The Euler system of Eq. (67) are discretised with the Spectral Difference (SD) method for unstructured spatial discretisation [22,24], using the formulation on quadrilateral grids discussed in [23]. Each quadrilateral cell constitutes an 'element' in which the coordinates are normalised. Within this element, the solved signal is reconstructed from n solution points with a degree $n-1$ polynomial for each coordinate direction. Similarly, degree n polynomials are used to reconstruct the fluxes of the transported variables from $n+1$ flux points. The Gauss-Legendre quadrature points are retained for locating the solution points, whereas the flux points are selected to be the Gauss-Legendre quadrature points of order $n-1$ plus the two ends points. This combination of quadrature points was shown by Jameson [24] to be linearly stable whatever the order of accuracy (i.e., the value of n) and also optimal for the reduction of aliasing errors and for providing good conditioning [24,28]. The reconstructed fluxes are only element-wise continuous, and discontinuous across the cell interfaces. A Riemann solver is applied to compute a common flux at cell interfaces, to ensure conservation and secure good stability. In the current work, the Roe solver with entropy fix is used [29,30]. The left and right states of the Riemann solver represent the solution on both sides of the shared edge flux point. Simulations are performed at the fifth order ($n = 5$).

The fourth-order, five-stage, strong stability preserving (RK45-SSP) scheme is adopted for time stepping [31].

Boundary conditions are enforced weakly using the same approach adopted for the numerical flux at the interior interfaces. For high-order discontinuous finite elements methods, such as the SD used in the present work, this approach is optimal and is often the preferred choice. Furthermore, the use of an approximate Riemann solver for the inviscid fluxes, which is characteristic by construction, guarantees well-posedness. In particular, to compute the numerical flux at the sonic outflow, the pressure, the density and the momentum are extrapolated from the interior of the domain.

The leading shock is captured over the mesh by applying a method designed to provide sub-cell resolution of the flow

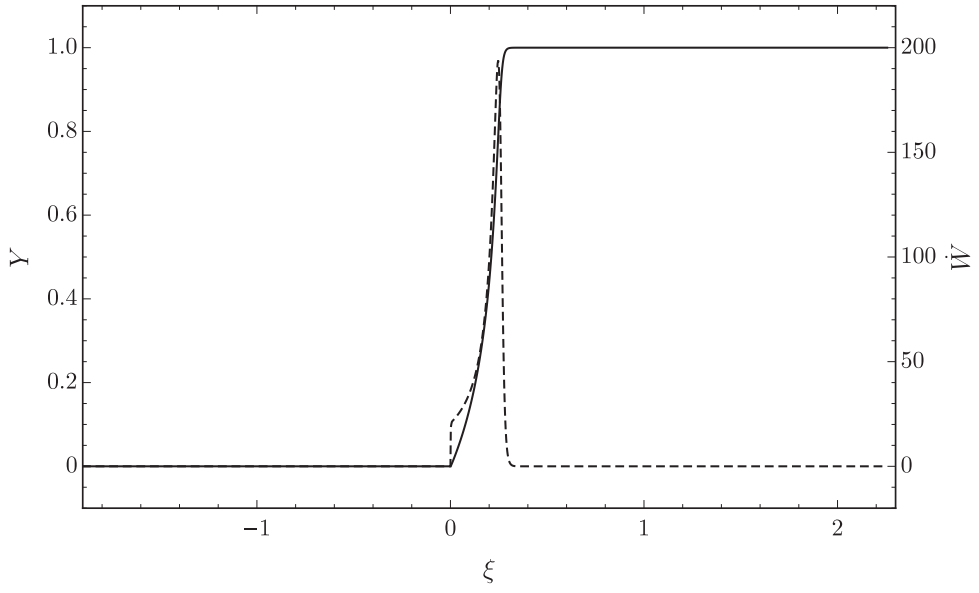

(a) Full domain

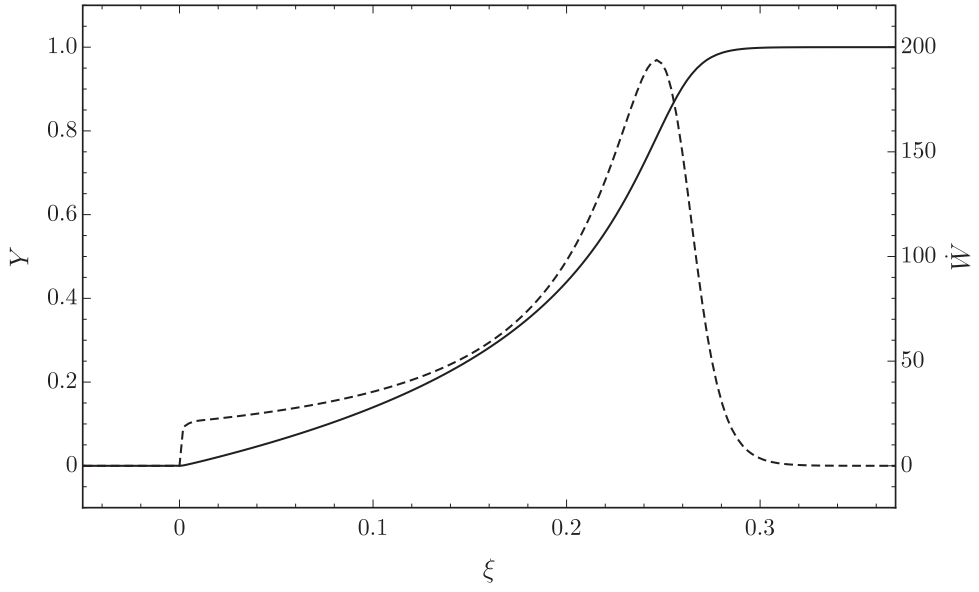

(b) Zoom into the detonation

Fig. 4. Distributions across a representative CJ steady detonation for $\gamma = 1.005$, $\epsilon = 0.1$, $\beta = 5$, $b = 0.9$: solid line, progress variable (left axis); dashed line, heat release rate $\dot{W}$ (right axis).

discontinuities through a high-order dissipation term added to all equations solved [32,33].[1] This well-established approach for shock capturing in the context of high-order methods is here coupled with a recently proposed modal sensor based on acoustic characteristics and density [26], in order to trigger the high-order dissipation term only where needed. This sensor makes use of the density and acoustic characteristics as the sensor variables, to allow for good resolution of shock discontinuities while partially mitigating post-shock oscillations [26]. The threshold and sensor tolerance are computed via a self calibration algorithm which determines the optimal values for these parameters for an arbitrary value of the order n from a manufactured solution, see [34] for the details on this calibration.

The number of solution points in the whole domain is 2000. The domain size for each simulation is set so that the detonation thickness is resolved over around 200 solution points.

[1] Notice that even though the leading shock is weak, solving the Navier-Stokes equations with physical viscosity instead of Euler with shock capturing was not found to be enough to stop the solution from diverging due to the fact that γ is very close to unity.

5.2.2. Scalar limiter

High-order methods are known to promote boundedness issues with scalar fields. Here, to secure perfect scalar boundedness, i.e.

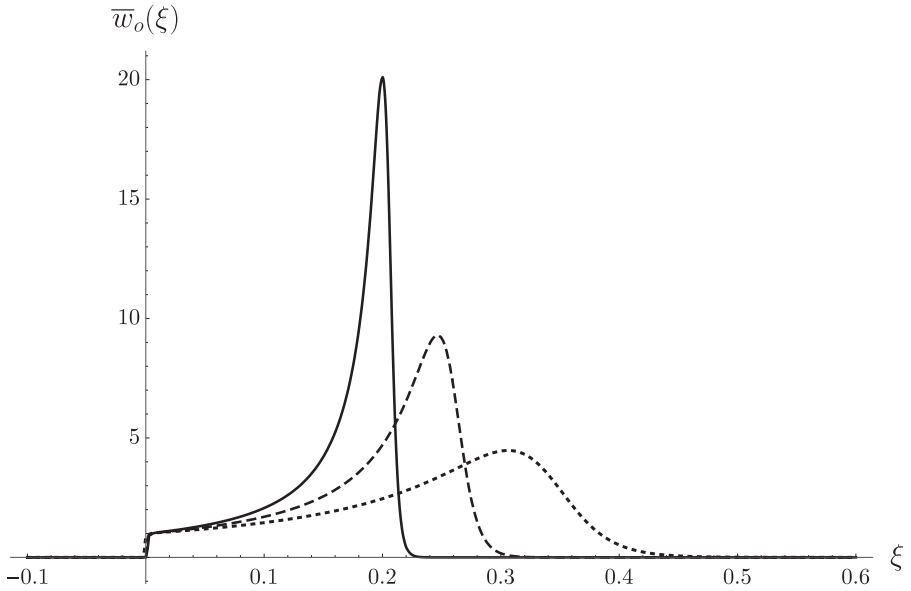

Fig. 5. Profiles of the reduced heat release rate for stable CJ detonations for $\beta = 6$ (solid line), $\beta = 5$ (dashed line), $\beta = 4$ (dotted line).

$Y \in [0, 1]$, a modified implementation of the positivity-preserving scheme introduced by Zhang and Shu [35] is adopted.[2]

Let the lower and upper bounds of Y be denoted as $B_L = \epsilon_Y$ and $B_U = 1 - \epsilon_Y$ respectively, where ϵ_Y is a small number (for instance, $\epsilon_Y = 10^{-13}$). Then, at each stage of the Runge-Kutta time-stepping process, we can define the parameter θ_Y over a standard element (computing cell) as

$$\theta_Y = \min\left(1, \frac{\overline{Y} - B_L}{\overline{Y} - Y_{min}}, \frac{B_U - \overline{Y}}{Y_{max} - \overline{Y}}\right), \tag{72}$$

where $\overline{Y}$ is the mean value of Y inside the element, and $Y_{\min}$ and $Y_{\max}$ are the minimum and maximum values of Y in the element respectively. The corrected value of Y is then calculated as

$$\hat{Y} = \theta_Y (Y - \overline{Y}) + \overline{Y}, \tag{73}$$

which will always be between B_L and B_U provided that $\overline{Y}$ is so.

It should be noted that we had to resort to limiting the non-conservative variable Y due to the limiting problem being ill-defined for the conservative variable ρY in the current implementation. As a consequence, the mean value of ρY will not be perfectly preserved over the element if ρ is not constant, and the limiter will act as a scalar source term. In practice the contribution of this source term stays negligible (on average it represents around 0.021% of the total mass of a fluid element) and cannot affect the overall quality of the solution.

5.2.3. Measurement of T_N

The burning rate as defined by Eq. (61) requires precise measurement of the instantaneous value of T_N, the Neumann temperature. T_N may be measured making use of the ZND structure of the detonation. Downstream of shock, the ZND profile for temperature is a quasi-linear function of the progress variable in the limit (19) and is given in [21] as

$$\frac{T - T_N}{T_u} = \epsilon^2 Y + \mathcal{O}[(\gamma - 1)\epsilon]. \tag{74}$$

Therefore, T_N can be obtained by measuring the value of T at two different values of $Y > 0$ downstream of the shock, and then by extrapolating linearly back to $Y = 0$. This approach is adopted in the current study with interpolation values for $Y \sim 10^{-2}$ to 10^{-1} depending on the mesh resolution. The process is repeated at each Runge-Kutta stage, and the method has been found to give sufficiently accurate measurements of T_N with a relative error in the order of 10^{-6}.

5.3. Steady CJ detonation

A reference steady CJ detonation is first computed for $\gamma = 1.005$, $\epsilon = 0.1$, $\beta = 5$, $b = 0.9$ and $\bar{t}_r = 0.048$. The length of the computational domain is about $4\bar{\ell}$, with the characteristic length $\bar{\ell} \equiv a_u \bar{t}_r$. Density and pressure are normalized by their upstream values, and velocity is normalized by $\sqrt{P_u/\rho_u}$. The corresponding distributions of these normalized primitive variables versus ξ, the non-dimensional coordinate defined by Eq. (16), are shown in Fig. 2 a with a zoom within the detonation zone in Fig. 2 b. The Neumann-state values of density, pressure and velocity exactly match those obtained from the ZND theory, Eq. (5), which hints to very low numerical dissipation at the shock.

Figure 3 shows the Mach number and speed of sound profiles across the inner structure of the detonation. It can be seen that the Mach number increases from around $1 - \epsilon = 0.9$ at the Neumann state to unity at the CJ point, thus validating the theoretical simplification of a transonic flow, and the two-time-scale nature of the dynamics. In addition, it can be seen that the variation in the speed of sound is of the order of ϵ^2, thus validating the theoretical simplification of a constant speed of sound.

Figure 4 a shows the progress variable and the heat release rate $\dot{W}$ featuring the cut-off towards fresh gases, Eq. (60). Looking at the zooms inside the detonation in Figs. 4 b and 2 b, it is confirmed that the combination of this cut-off temperature in the burning rate with the high-order shock capturing approach minimizes the spurious leaking of mass and heat within the leading shock (i.e., for $\xi < 0$).

6. Comparison of theory against simulations

In order to compare the theoretical predictions from Section 3 with the numerical counterparts, the stability of detonations is studied for different values of $\beta \in [2, 8]$. In particular, the transition activation energy, b^*, and the corresponding oscillation

[2] Note that the high-order dissipation term is not triggered outside of the leading shock, therefore the reaction zone and the progress variable profile are free from additional dissipation.

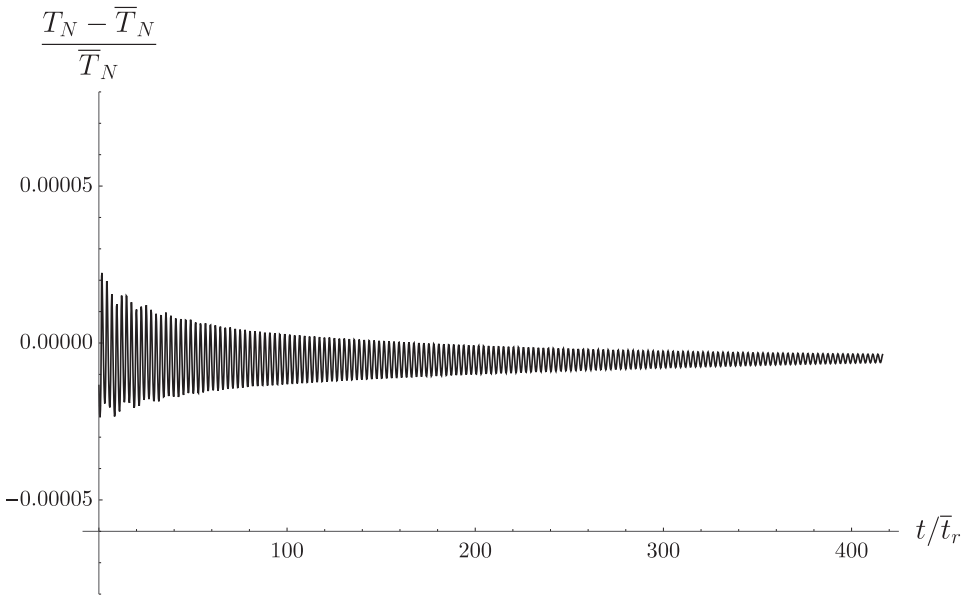

(a) $b = 1.15$

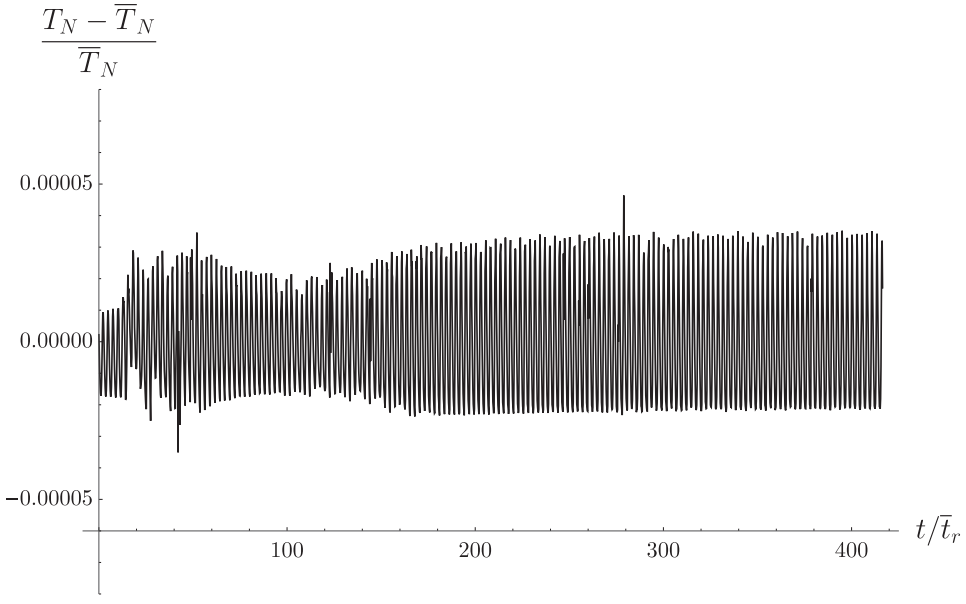

(b) $b = 1.23$

Fig. 6. Normalized Neumann temperature versus time for detonations at $\beta = 5$, with stability threshold $b^* = 1.21$ (a) return to a steady CJ; (b) unstable detonation.

frequency, ω^*, as a function of β are used to verify consistency in the results.

The theoretically expected values of these quantities can be obtained from the asymptotic stability analysis as follows: the evolution Eq. (65) is first integrated to obtain $\overline{Y}_\beta(\xi)$, which is used to calculate $\overline{w}_{o\beta}(\xi) = [1 - \overline{Y}_\beta(\xi)]e^{\beta \overline{Y}_\beta(\xi)}$. Hence, the reaction rate $\overline{w}_{o\beta}(\xi)$ is used to calculate $\overline{\mu}(\xi)$ from Eq. (43), such that $\overline{w}_{o\beta}$ and $\overline{\mu}$ can both be used to calculate $g(\zeta)$ from Eqs. (53) and (47). Finally, $g(\zeta)$ is used to obtain the theoretically predicted values of b^* and ω^* from Eq. (56).

To check consistency with numerical results issued from the integration of the Euler equations, two different procedures are adopted:

- Stable CJ detonations are computed numerically for different selected values of β within the range of interest. The reduced heat release rate profiles $\overline{w}_o(\xi)$ are extracted from the relevant distribution of the progress variable (cf. Eq. 65). Figure 5 shows the reduced heat release rate profile $\overline{w}_o(\xi)$ for stable detonations at various reduced activation energies β, as obtained from numerical simulations. The critical activation energy b^* and the corresponding oscillation frequency ω^* at the instability threshold are then obtained from theory via Eqs. (53)–(56) in the limit for $\overline{w}_o(\xi) \to w_{o\beta}(\xi)$. The relevant results from this procedure, which makes use of a blend of theory and numerics, will be hereafter referred to as "Theory, Numerical $\overline{w}$" (TN$\overline{w}$).
- The second procedure relies solely on the numerical solution of the Euler equations. In particular, a reference CJ detonation

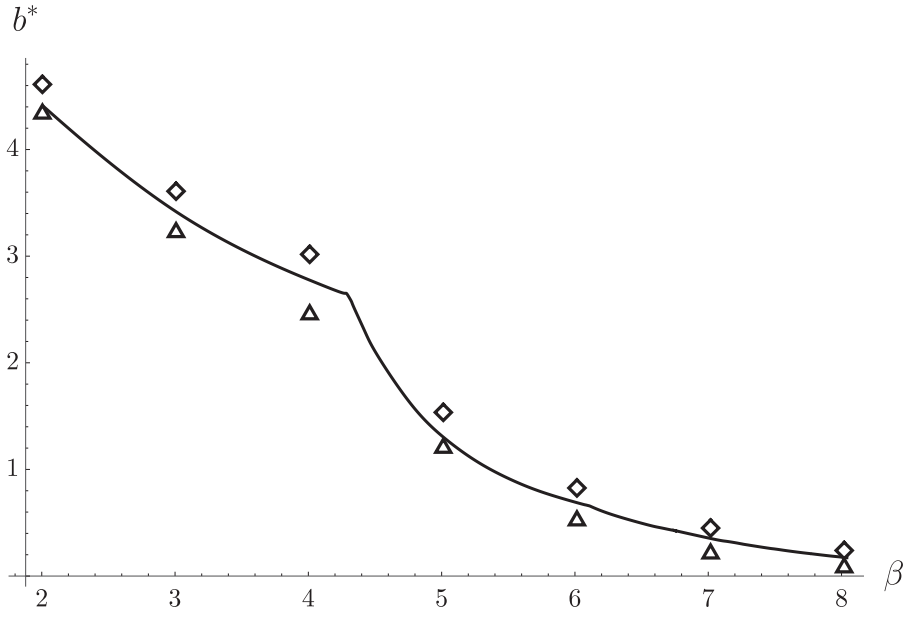

(a) Critical activation energy

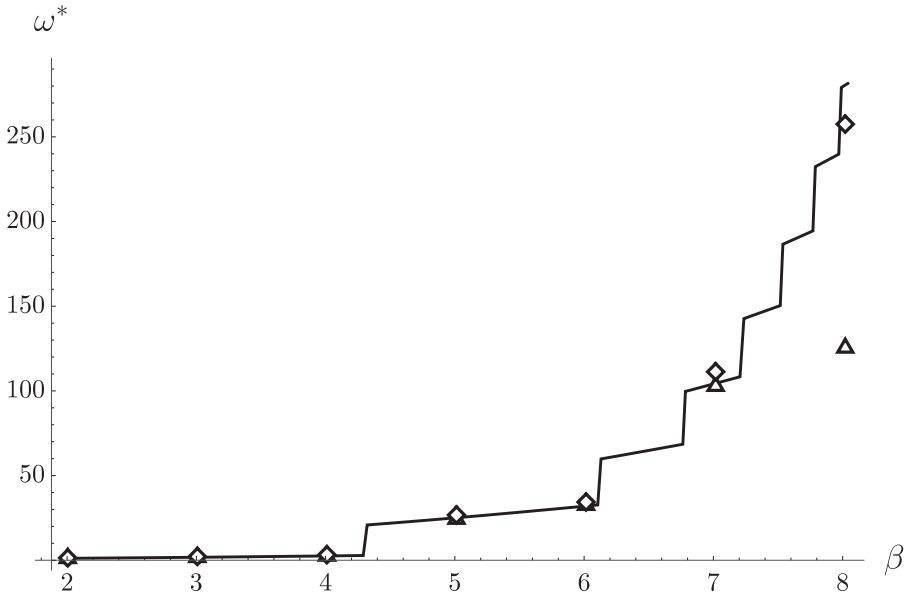

(b) Critical oscillation frequency

Fig. 7. Comparison between theory and simulation: solid line, theory; triangles, SIM; diamonds, TN$\overline{w}$.

for a given b is used to initialise subsequent simulations at different values of b and a fixed value of β. The Neumann temperature is collected versus time, restarting the simulation for $b < b^*$ the solution evolves towards a steady CJ detonation, for $b > b^*$ periodic oscillations are observed. As shown, for instance, in Fig. 6, for b approaching its threshold instability value, the simulation very slowly returns toward a steady CJ case (Fig. 6 a), while for b above its threshold, the temperature oscillation is sustained (Fig. 6 b). Accordingly, the values of b^* and ω^* are determined by a trial-and-error procedure checking the onset of the instability on the time evolution of T_N. Since the oscillation period is expected to be of order of t_r/ϵ with $\epsilon = \sqrt{q_m/c_p T_u} = 0.1$, the runtime for each of the simulations is set in the order of $10^3 t_r$ to allow sufficient convergence of the results. This procedure will be referred to as "SIM".

The transition activation energy b^* and the corresponding oscillation frequency ω^* as obtained from the theory and the two numerical procedures SIM and TN$\overline{w}$ are plotted against the reaction-zone activation energy β in Fig. 7a and b, respectively. The results show that the transition activation energy b^* decreases with increasing β, consistent with the observation that the detonation becomes stiffer and thus more unstable with increasing β (cf. Fig. 5). Oscillation frequency on the other hand increases with increasing β.

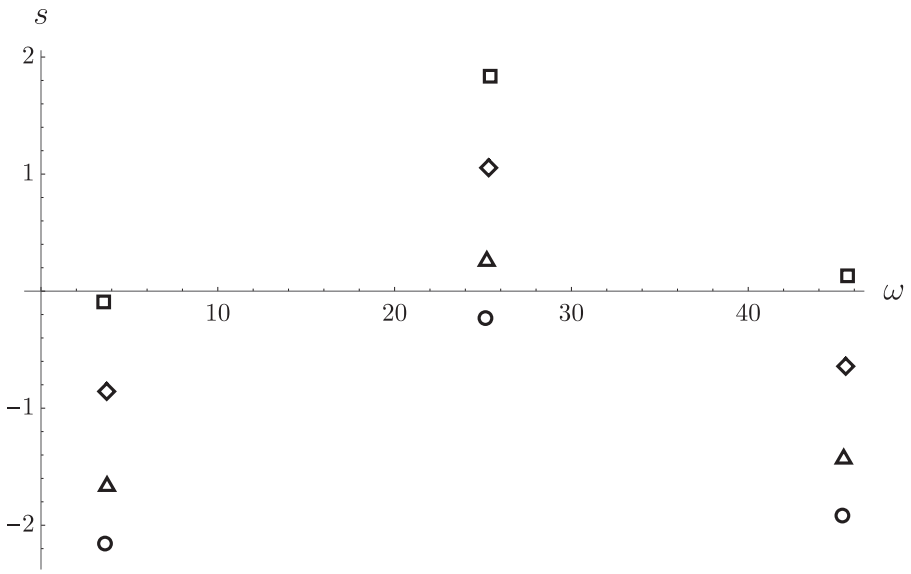

Fig. 8. Growth rate s of the first three oscillation modes at different values of activation energy b for the detonation with $\beta = 5$: circles, $b = 1.2$; triangles, $b = 1.4$; diamonds, $b = 1.8$; squares, $b = 1.2$. It can be seen that the second mode is the most unstable.

The breaks in the b^* curve and the corresponding jumps in the ω^* curve are due to the existence of multiple oscillation modes for the detonation. By fixing the value of b and solving Eq. (55) for the growth rate s and oscillation frequency ω, a frequency spectrum of the detonation oscillations can be obtained. As shown in Fig. 8, different oscillation modes exist for a detonation, and for $\beta = 5$, the second mode is the most unstable one, transitioning to instability at some value of $1.2 < b < 1.4$. The third mode becomes unstable for some b slightly less than 2.3, while the first mode is still stable at $b = 2.3$. The most unstable mode changes with β, which leads to the jumps in ω^* observed in Fig. 7b.

The results show a very good agreement between numerical and theoretical values for both b^* and ω^*. For large values of β, the solution using the numerical burning rate is in better agreement with the theory than the simulation. Two reasons may be put forward to explain this observation. First, the asymptotic analysis assumes a frequency of order unity, thus the quality of the results may be expected to degrade when the frequency of the oscillation increases. Second, for large values of β, the transition to chaos occurs within a very small interval of the parameter b which makes the trial-and-error determination of b^* and ω^* much less accurate.

7. Conclusion

High-order numerical simulations and asymptotic developments have been used to tackle the dynamics of one-dimensional gaseous detonations in the limit of low heat released coupled with the Newtonian approximation. The focus was on the stability thresholds in terms of activation energy controlling detonations in the Chapman-Jouguet regime. Simulations were performed using a 5th order accurate spectral difference discretization solving the inviscid Euler balance equations, combined with a recently developed high-order shock capturing approach based on characteristic waves sensors. This numerical strategy combined with a specific Arrhenius expression for chemistry allows for the separation of the leading shock from the downstream reaction zone, thus limiting the impact of spurious numerical diffusion of heat and mass ahead of the shock.

In the theoretical part, the time-dependent velocity of the shock appears as the eigenfunction of a single hyperbolic equation for the flow velocity, namely Eq. (42), and the solution is expressed in terms of an integral equation for the shock velocity. The threshold levels of activation energy at which the instability occurs obtained from the theory are in very good agreement with those obtained from numerical simulations.

The theory is grounded on the existence of fast downstream running waves and slow upstream running waves, both traveling between the reaction zone and the shock. The disturbances originating from the downstream running waves are considered to be quasi-instantaneous. An unstable detonation is observed for conditions at which the upstream running wave is in phase with the shock oscillations. The corresponding oscillation frequencies also agree well between theory and numerical predictions.

In order to further substantiate the generic character of the results reported in this study, future work shall focus on the validity of such theoretical predictions away from the Newtonian and low heat-release limits.

Declaration of Competing Interest

The authors declare that they have no known competing financial interests or personal relationships that could have appeared to influence the work reported in this paper.

Acknowledgments

This work is supported by ANR (Agence Nationale de la Recherche) under the project 18-CE05-0030 'ReDDT' (Revisiting Deflagration to Detonation Transition in the context of carbon-free energy production).

References

[1] J.J. Erpenbeck, Stability of steady-state equilibrium detonations, Phys. Fluids 5 (5) (1962) 604–614.
[2] W. Fickett, W.W. Wood, Flow calculations for pulsating one-dimensional detonations, Phys. Fluids 9 (5) (1966) 903–916.
[3] J.H. Lee, The Detonation Phenomenon, Cambridge University Press, Cambridge, 2008.
[4] E.S. Oran, Understanding explosions – from catastrophic accidents to creation of the universe, Proc. Combust. Inst. 35 (1) (2015) 1–35.
[5] S.W. Grib, C.A. Fugger, .P.S. Hsu, N. Jiang, S. Roy, S.A. Schumaker, Two-dimensional temperature in a detonation channel using two-color OH planar laser-induced fluorescence thermometry, Combust. Flame 228 (2021) 259–276.

[6] P. Honhar, C.R. Kaplan, R.W. Houim, E.S. Oran, Role of reactivity gradients in the survival, decay and reignition of methane-air detonations in large channels, Combust. Flame 222 (2020) 152–169.
[7] J. Melguizo-Gavilanes, V. Rodriguez, P. Vidal, R. Zitoun, Dynamics of detonation transmission and propagation in a curved chamber: a numerical and experimental analysis, Combust. Flame 223 (2021) 460–473.
[8] C.A. Towery, A.Y. Poludnenko, P.E. Hamlington, Detonation initiation by compressible turbulence thermodynamic fluctuations, Combust. Flame 213 (2020) 172–183.
[9] J.C. Schulz, K.C. Gottiparthi, S. Menon, Ionization in gaseous detonation waves, Shock Waves 22 (2012) 579–590.
[10] Y. Morii, A.K. Dubey, H. Nakamura, K. Maruta, Two-dimensional laboratory-scale DNS for knocking experiment using n-heptane at engine-like condition, Combust. Flame 223 (2021) 330–336.
[11] Z. Rui, W. Dan, W. Jianping, Progress of continuously rotating detonation engines, Chin. J. Aeronaut. 29 (1) (2016) 15–29.
[12] Y. Uemura, A.K. Hayashi, M. Asahara, N. Tsuboi, E. Yamada, Transverse wave generation mechanism in rotating detonation, Proc. Combust. Inst. 34 (2) (2013) 1981–1989.
[13] Z. Pan, B. Fan, X. Zhang, M. Gui, G. Dong, Wavelet pattern and self-sustained mechanism of gaseous detonation rotating in a coaxial cylinder, Combust. Flame 158 (11) (2011) 2220–2228.
[14] E.M. Braun, F.K. Lu, D.R. Wilson, J.A. Camberos, Airbreathing rotating detonation wave engine cycle analysis, Aerospace Sci. Technol. 27 (1) (2013) 201–208.
[15] V. Anand, E. Gutmark, Rotating detonation combustors and their similarities to rocket instabilities, Prog. Energy Combust. Sci. 73 (2019) 182–234.
[16] K. Matsuoka, M. Tanaka, T. Noda, A. Kawasaki, J. Kasahara, Experimental investigation on a rotating detonation cycle with burned gas backflow, Combust. Flame 225 (2021) 13–19.
[17] P. Clavin, Nonlinear dynamics of shock and detonation waves in gases, Combust. Sci. Technol. 189 (5) (2017) 747–775.
[18] P. Clavin, G. Searby, Combustion Waves and Fronts in Flows: Flames, Shocks, Detonations, Ablation Fronts and Explosion of Stars, Cambridge University Press, 2016.
[19] P. Clavin, B. Denet, Analytical study of the direct initiation of gaseous detonations for small heat release, J. Fluid Mech. 897 (2020). A30
[20] P. Clavin, R. Hernández-Sánchez, B. Denet, Asymptotic analysis of the critical dynamics of spherical gaseous detonations, J. Fluid Mech 915 (2021). A122
[21] P. Clavin, F.A. Williams, Dynamics of planar gaseous detonations near Chapman-Jouguet conditions for small heat release, Combust. Theory Model. 6 (1) (2002) 127–139.
[22] D.A. Kopriva, J.H. Kolias, A conservative staggered-grid Chebyshev multidomain method for compressible flows, J. Comput. Phys. 125 (1) (1996) 244–261.
[23] Y. Sun, Z. Wang, Y. Liu, High-order multidomain spectral difference method for the Navier-Stokes equations on unstructured hexahedral grids, Com. Comput. Phys. 2 (2) (2007) 310–333.
[24] A. Jameson, A proof of the stability of the spectral difference method for all orders of accuracy, J. Sci. Comput. 45 (2010) 348–358. 1–3
[25] P. Clavin, L. He, Stability and nonlinear dynamics of one-dimensional overdriven detonations in gases, J. Fluid Mech. 306 (1996) 353–378.
[26] G. Lodato, Characteristic modal shock detection for discontinuous finite element methods, Comput. Fluids 179 (2019) 309–333.
[27] W. Fickett, W.C. Davis, Detonation: Theory and Experiment, Courier Corporation, 2000.
[28] A. Jameson, P. Vincent, P. Castonguay, On the non-linear stability of flux reconstruction schemes, J. Sci. Comput. 50 (2) (2012) 434–445.
[29] P.L. Roe, Approximate Riemann solvers, parameter vectors, and difference schemes, J. Comput. Phys. 43 (2) (1981) 357–372.
[30] A. Harten, High resolution schemes for hyperbolic conservation laws, J. Comput. Phys. 49 (3) (1983) 357–393.
[31] R.J. Spiteri, S.J. Ruuth, A new class of optimal high-order strong-stability-preserving time discretization methods, SIAM J. Numer. Anal. 40 (2) (2002) 469–491.
[32] P.-O. Persson, J. Peraire, Sub-cell shock capturing for discontinuous Galerkin methods, AIAA Proc. (2006) 1–13. 2006-112
[33] P.O. Persson, Shock capturing for high-order discontinuous Galerkin simulation of transient flow problems, AIAA Proc. (2013) 1–9. 2013–3061
[34] G. Lodato, L. Vervisch, P. Clavin, Direct numerical simulation of shock wavy-wall interaction: analysis of cellular shock structures and flow patterns, J. Fluid Mech. 789 (2016) 221–258.
[35] X. Zhang, C.W. Shu, On positivity-preserving high order discontinuous Galerkin schemes for compressible euler equations on rectangular meshes, J. Comput. Phys. 229 (23) (2010) 8918–8934.